

**Mechanical strength and electronic instabilities in ultra-incompressible platinum dinitrides**R. F. Zhang,<sup>1,2,\*</sup> D. Legut,<sup>3</sup> Z. H. Fu,<sup>1</sup> S. Veprek,<sup>4</sup> Q. F. Zhang,<sup>1</sup> and H. K. Mao<sup>5</sup><sup>1</sup>*School of Materials Science and Engineering, and International Research Institute for Multidisciplinary Science, Beihang University, Beijing 100191, People's Republic of China*<sup>2</sup>*Theoretical Division, Los Alamos National Laboratory, Los Alamos, New Mexico 87545, USA*<sup>3</sup>*IT4Innovations Center, VSB-Technical University of Ostrava, CZ-708 33 Ostrava, Czech Republic*<sup>4</sup>*Department of Chemistry, Technical University Munich, Lichtenbergstrasse 4, D-85747 Garching, Germany*<sup>5</sup>*Geophysical Laboratory, Carnegie Institution of Washington, NW Washington, D.C. 20015, USA*  
*and Center for High Pressure Science and Technology Advanced Research, Pudong, Shanghai 201203, People's Republic of China*  
(Received 26 June 2015; published 16 September 2015)

The mechanical properties and electronic structure of recently synthesized PtN<sub>2</sub>, proposed as a potential candidate for superhard materials, have been investigated by means of density functional theory. Although it shows a clear band gap indicating a covalent bonding nature, the calculated shear moduli and ideal strengths of both proposed PtN<sub>2</sub> polymorphs are much lower than those of ReB<sub>2</sub>, suggesting that it should be weaker than ReB<sub>2</sub>, whose load-invariant hardness is less than 30 GPa. The anisotropic strength of the pyrite PtN<sub>2</sub> polymorph is significantly higher than that of the fluorite polymorph due to a larger covalent contribution. The shear instability for both polymorphs occurs in a cleavagelike mode between the weakly bonded crystal planes. This behavior is different from transition-metal (TM) diborides where the TM-TM or TM-B bonds are the carriers of the shear instability.

DOI: [10.1103/PhysRevB.92.104107](https://doi.org/10.1103/PhysRevB.92.104107)

PACS number(s): 62.20.de, 61.50.Ah, 62.20.M-, 71.20.Ps

**I. INTRODUCTION**

Noble transition metals (TMs) (Pt, Pd, Ir, Os, Ru, and Rh) were thought not to form nitrides [1,2], but several such compounds have been synthesized recently under the conditions of high pressure and temperature [3–5]. The follow-up studies of their structure and mechanical properties evoked significant interest in the possibility to synthesize such compounds and in their potential applications [6–15]. This work has been motivated by the concept proposed by Kaner *et al.* [16,17] who suggested synthesizing superhard materials by introducing light elements, such as boron, carbon, nitrogen, or oxygen, into transition metals that have high elastic moduli [16–18]. Accordingly, the high density of the valence electrons of transition metals should provide such compounds with high stiffness, and the covalent bonds between transition metals and nonmetal elements should enhance the resistance against plastic deformations.

Since its first discovery, PtN<sub>2</sub> has been expected to be a candidate as a potential superhard solid because it possesses a high bulk modulus of 372(±5) GPa [3–5] comparable to that of the superhard cubic-BN (c-BN) (bulk modulus = 370 GPa, hardness ≈48 GPa [19]). The drawback of this concept is the fact that high elastic moduli do not guarantee high hardness because electronic instability and transformations to softer phases may occur upon large shear strain at the atomic level under fully developed plastic flow where the correct load-invariant hardness has to be measured (see, e.g., Ref. [20] and references therein).

On the basis of the concept of Kaner *et al.*, borides of TMs, TMB<sub>2</sub> (TM = Os, Re [17,21–23]), and TMB<sub>3</sub> (TM = W, Mo [24–27]) have been synthesized recently. However, although they possess high elastic moduli, the load-invariant hardnesses of ReB<sub>2</sub>, OsB<sub>2</sub>, and WB<sub>3</sub> are below 30 GPa. This

is in agreement with the calculated ideal strengths of ReB<sub>2</sub>, OsB<sub>2</sub>, and WB<sub>3</sub> which are much lower than those of c-BN [22,23,26,28,29]. Recent theoretical studies indicate that the bonds between TM-B are responsible for the lattice instability of WB<sub>3</sub> and ReB<sub>2</sub> under shear deformation [26,28], whereas the weak TM-TM bonds contribute to the shear sliding in OsB<sub>2</sub> [23]. The weakness and lattice instability of these borides are attributed to the appearance of metallic bonds. Therefore, much interest arose to find transition-metal borides, nitrides, or carbides with predominantly covalent bonds that show a distinct band gap. After an exploration of several borides and nitrides we found that PtN<sub>2</sub> meets this requirement because the pyrite phase shows a distinct band gap of about 1.8 eV (see below). Therefore the question arises if PtN<sub>2</sub> can be superhard. In the present studies we show that the weak Pt-N bonds limit the ideal strengths of PtN<sub>2</sub>. During shear, a unique cleavagelike mode of lattice instability is found to be attributed to the weak bonds between the {100} and the {111} planes in the pyrite- and fluorite-type polymorphs, respectively.

In the early days, the ideal tensile (decohesion) and shear strengths were roughly estimated as  $(\gamma_S E_Y / d_0)^{0.5} \approx 0.1 E_Y$  and  $G a / (2\pi d_0) \approx 0.1 G$ , respectively [30,31] ( $G$  and  $E_Y$  are the shear and Young's modulus,  $\gamma_S$  is the surface energy,  $a$  is the interatomic distance in the shear direction, and  $d_0$  is the interplanar spacing). Recent advances in computational techniques have made it possible to calculate the ideal strengths in a quantitative way by means of density functional theory, which provides a unique way to analyze the bond deformation paths and electronic instabilities under various loadings [23,26,28]. Although the ideal shear strength correlates with the onset of dislocation formation and plastic deformation in an ideal crystal [32–34], the strength of a real material is generally limited by flaws, such as dislocations, microcracks, grain boundaries, and others, and it is usually orders of magnitude smaller than the ideal one. Nevertheless, a correlation between Peierls-Nabarro (PN) stress of dislocations and ideal shear strength has also been quantified via the PN model [35–37]

\*Corresponding author: [zrf@buaa.edu.cn](mailto:zrf@buaa.edu.cn)

as  $\tau_p = K \exp(-\alpha\zeta/b)$ , where  $\alpha = 2\pi$ ,  $K = G/(1 - \nu)$  for edge dislocation,  $K = \mathbf{G}$  for screw dislocation,  $b$  is the Burgers vector,  $\nu$  is the Poisson ratio, and  $\zeta$  is the dislocation half-width which can be expressed as  $\zeta = Kb/4\pi\tau_{\max}$ , where  $\tau_{\max}$  is the ideal shear strength. Thus, the plastic resistance of a crystal depends mostly on two intrinsic mechanical parameters: shear modulus  $G$  and ideal shear strength  $\tau_{\max}$ .

## II. COMPUTATIONAL METHOD

Our first-principles calculations were performed by means of the Vienna *ab initio* simulation package (VASP) code [38] using density functional theory with the projector augmented-wave (PAW) method [39] employed to describe the electron-ion interaction. In order to avoid a possible artifact due to the choice of the potential, both PAW-LDA (local density approximation) and PAW-PBE (Perdew-Burke-Ernzerhof) potentials [40] have been used for the exchange-correlation term in our calculations. The integration within the Brillouin zone was performed according to the Monkhorst-Pack scheme and the tetrahedron method with Blöchl corrections for the energy and electronic calculation and Gaussian smearing for the stress calculations, respectively. The conjugate gradient method was used for the relaxation of structural parameters.

As a further check of the validity of the applied PAW-LDA and PAW-PBE potentials, we determine the elastic constants and moduli by applying a set of small deformations  $\delta$  between  $-0.02$  and  $+0.02$ , and calculating the second-order coefficients in a polynomial fit of the total energy as a function of the distortion  $\delta$ . The applied strain configurations and the corresponding strain-energy density variations  $\Delta E/V_0$  are given as follows: (c1)  $\varepsilon = (\delta, 0, 0, 0, 0, 0)$  where  $\Delta E/V_0 \approx \frac{1}{2}C_{11}\delta^2$ , (c2)  $\varepsilon = (0, 0, 0, \delta, 0, 0)$  where  $\Delta E/V_0 \approx \frac{1}{2}C_{44}\delta^2$ , and (c3)  $\varepsilon = (\delta, \delta, \delta, 0, 0, 0)$  where  $\Delta E/V_0 \approx \frac{3}{2}(C_{11} + 2C_{12})\delta^2$ .

The phonon calculations were performed within the harmonic approximation using the direct method [41] based on the calculated nonvanishing Hellman-Feynman forces employing the PHONOPY code [42]. To confirm our results, we also used a linear-response method based on the perturbation theory as implemented in the recent version of the VASP code.

In the calculation of stress-strain relationships, the atomic basis vectors of a given crystal cell were first projected onto the Cartesian coordinates with one axis vector being parallel to the imposed strain direction for the tension. For the shear, one axis vector was perpendicular to the slip plane, and another one was parallel to the slip direction on that plane. Afterwards, the crystal has been incrementally deformed by transforming the unstrained atomic basis vector matrices to the strained ones using the deformation matrices. In order to keep the crystal under a stress state of uniaxial tension or shear, the strained cell has been relaxed for both the atomic basis vectors and the atom coordinates inside the unit cell by keeping the applied strain component fixed and relaxing the other five strain components until their conjugate stress components, i.e., Hellmann-Feynman stresses, reached negligible values. Such a relaxation scheme is accomplished by the slightly modified VASP code with specific constraints of strain components. To ensure that the strain path is continuous, the starting position at each strain step has been taken from the relaxed coordinates of the previous strain step. In the case of a large strain, the crystal

symmetry may be changed and the Brillouin zone significantly deformed. Therefore we adopt a high-energy cutoff of 600 eV and verified the convergence of the calculations of the stress-strain curves by using different meshes of  $k$  points. The method of calculation has also been described and thoroughly checked in our previous papers [43–45] to which we refer for further details.

## III. RESULTS AND DISCUSSION

The composition and structure of  $\text{PtN}_2$  have been investigated by several groups both experimentally and theoretically [3,5,6,11]. The stoichiometry of  $\text{PtN}_2$  has been experimentally confirmed recently [5], but the crystal structure of pyrite and fluorite polymorphs are the subject of intense studies [6,11,46]. The pyrite structure of  $\text{PtN}_2$  (P- $\text{PtN}_2$ ), shown in Fig. 1(a), can be described as a rock-salt structure in which the Pt atoms occupy the fcc sites, and the  $\text{N}_2$  dimers are in the fcc octahedral interstitial sites oriented in all four possible  $\langle 111 \rangle$  directions. The Pt-6N octahedron shares its edges with the neighboring tetrahedron, and each N atom is tetrahedrally bonded to another N atom and three Pt atoms [see Fig. 1(c)]. The alternate fluorite  $\text{PtN}_2$  (F- $\text{PtN}_2$ ), suggested by Yu and Zhang [47], is shown in Fig. 1(b). In this structure, all N atoms occupy the

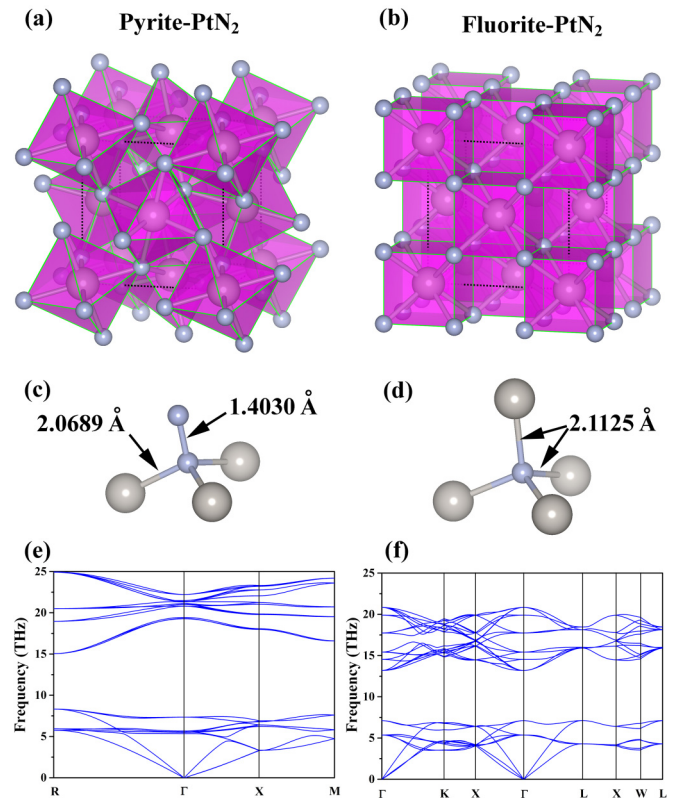


FIG. 1. (Color online) Lattice topology and polyhedra of the (a) pyrite (P-) and (b) fluorite (F-)  $\text{PtN}_2$ . In each polyhedron, one Pt cation is bonded to six N anions for pyrite and eight N anions for fluorite structures, respectively. The arrangements and lengths of the bonds between N atoms and their neighbors for (c) P- $\text{PtN}_2$  and (d) F- $\text{PtN}_2$ . The large and small spheres represent the Pt and N atoms, respectively. Calculated phonon dispersion curves for (e) pyrite and (f) fluorite structures.

TABLE I. The equilibrium lattice parameter  $a$  (Å), elastic constants  $C_{ij}$  (GPa), Poisson ratio  $\nu = (3B_v - 2G_v)/(6B_v + 2G_v)$ , isotropic Voigt bulk modulus  $B_v = (C_{11} + 2C_{12})/3$  (GPa) and shear modulus  $G_v = (3C_{44} + C_{11} - C_{12})/5$  (GPa) compared with previous studies for P-PtN<sub>2</sub> and F-PtN<sub>2</sub>. The values given in parentheses are from PAW-PBE potentials.

	P-PtN <sub>2</sub>		F-PtN <sub>2</sub>	
	Present	Previous	Present	Previous
$a$	4.785(4.866)	4.77(4.86) <sup>a</sup> 4.79(4.875) <sup>b</sup>	4.877(4.962)	4.866(4.958) <sup>c</sup>
$C_{11}$	819.9(697.4)	824(668) <sup>a</sup>	527.1(452.0)	532(457) <sup>c</sup>
$C_{12}$	116.8(79.5)	117(78) <sup>a</sup>	208.5(172.2)	208(167) <sup>c</sup>
$C_{44}$	145.8(132.4)	152(133) <sup>a</sup>	114.8(94.3)	122(99) <sup>c</sup>
$\nu$	0.233(0.213)	0.247(0.226) <sup>a</sup>	0.315(0.314)	0.32(0.31) <sup>c</sup>
$B_v$	351.2(285.5)	352(272) <sup>a</sup> 347(278) <sup>b</sup>	314.7(265.5)	316(264) <sup>c</sup>
$G_v$	228.1(203.0)	214(184) <sup>a</sup>	132.6(112.5)	137(116) <sup>c</sup>

<sup>a</sup>Reference [46].

<sup>b</sup>Reference [5].

<sup>c</sup>Reference [47].

tetrahedral interstitial sites in the fcc-Pt lattice, and each Pt-8N polyhedron shares its edges with the neighboring tetrahedrons. Accordingly, each N atom is tetrahedrally bonded to four neighbor Pt atoms [see Fig. 1(d)].

Both F-PtN<sub>2</sub> and P-PtN<sub>2</sub> were relaxed with respect to lattice parameters and atom positions. The resulting parameters, listed in Table I, compare well with the experimental and theoretical values reported by other researchers [5,46,47]. The Pt-N bond lengths of 2.0689 Å in P-PtN<sub>2</sub> are shorter than those in F-PtN<sub>2</sub> (2.1125 Å), indicating stronger bonds for the former. Based on the reaction  $\text{Pt} + \text{N}_2 = \text{PtN}_2$ , the formation energy was calculated as  $\Delta E = 1/3[E(\text{PtN}_2) - E(\text{Pt}) - E(\text{N}_2)]$  with N<sub>2</sub> and Pt in their ground states. The resulting formation energies for P-PtN<sub>2</sub> and F-PtN<sub>2</sub>, obtained from PAW-LDA potentials, are  $-0.981$  and  $-0.919$  eV/atom, respectively. Thus, P-PtN<sub>2</sub> is thermodynamically more stable than F-PtN<sub>2</sub>. In the following parts, we will show that the choice of different lattice topologies, i.e., the occupation sites of N atoms in the fcc-Pt lattice, results in significantly different electronic properties of P-PtN<sub>2</sub> and F-PtN<sub>2</sub>. It will be shown that these differences are the physical origin of the different mechanical properties of both polymorphs.

The calculated phonon dispersion relations and phonon density of states (PDOS) were the same as those using the  $2 \times 2 \times 2$  supercell method. Figures 1(e) and 1(f) show the phonon dispersion relations of P-PtN<sub>2</sub> and F-PtN<sub>2</sub> which confirm the dynamic stability of both structures as there are no imaginary modes (negative frequencies). The lower frequencies of the PDOS are dominated by lattice dynamics of heavy Pt atoms and the higher frequencies by light N atoms.

The resulting structural parameters and elastic properties of PtN<sub>2</sub> in pyrite and fluorite structures are presented in Table I together with the available theoretical values from the literature [5,46,47]. The calculated elastic properties are in agreement with the previous theoretical values, thus showing the reliability of our calculations. The elastic constants of both crystal structures satisfy the Born stability criteria of

a cubic crystal:  $C_{44} > 0$ ,  $C_{11} > C_{12} > 0$  and  $C_{11} + 2C_{12} > 0$ , thus confirming that both structures of PtN<sub>2</sub> are mechanically stable. The calculated bulk modulus [351 GPa (LDA), 286 GPa (PBE)] of P-PtN<sub>2</sub> is slightly higher than that of F-PtN<sub>2</sub> [315 GPa (LDA), 266 GPa (PBE)]. Both bulk moduli from PAW-LDA and PAW-PBE potentials are higher than 250 GPa, suggesting that both PtN<sub>2</sub> polymorphs are ultraincompressible solids.

The shear modulus of 228 GPa (LDA) and 203 GPa (PBE) is much larger than that of the pure Pt metal [ $\sim 61$  GPa (PBE)]. The critical value of the ratio of shear modulus  $G$  to bulk modulus  $B$  of about 0.57 separates ductile ( $G/B < 0.57$ ) and brittle ( $G/B > 0.57$ ) materials [48]. For P-PtN<sub>2</sub> this ratio is between 0.65 (LDA) and 0.71 (PBE), and for F-PtN<sub>2</sub> it is between 0.62 (LDA) and 0.42 (PBE). Thus P-PtN<sub>2</sub> is expected to be brittle, whereas F-PtN<sub>2</sub> is close to the boundary between brittle and ductile because the PAW-PBE and PAW-LDA potentials yield too different values.

Next we determine the ideal tensile (decohesion) and shear strengths by calculating the stress-strain relationships for different types of loading. Figure 2 shows the stress-strain curves calculated for P-PtN<sub>2</sub> [Fig. 2(a) for PAW-PBE potentials and Fig. 2(b) for PAW-LDA potentials] in comparison with F-PtN<sub>2</sub> [Fig. 2(c) for PAW-PBE potentials and Fig. 2(d) for PAW-LDA potentials]. Taking PAW-LDA potentials as an example, the anisotropy ratio of the ideal tensile strengths of P-PtN<sub>2</sub> is  $\sigma_{[111]} = 52 \text{ GPa} : \sigma_{[110]} = 46 \text{ GPa} : \sigma_{[100]} = 40 \text{ GPa} \approx 1.3 : 1.2 : 1$ , which is much lower than that of F-PtN<sub>2</sub>  $\sigma_{[100]} = 60 \text{ GPa} : \sigma_{[110]} = 35 \text{ GPa} : \sigma_{[111]} = 22 \text{ GPa} \approx 2.7 : 1.6 : 1$ , indicating the nearly isotropic nature of the tensile strengths for P-PtN<sub>2</sub>. The PAW-PBE potentials provide similar results. On the contrary, the ideal tensile strengths of F-PtN<sub>2</sub> along the [100] directions of about 60 GPa are much larger than in the other two directions. The weakest direction along [100] with an ideal tensile strength of 40 GPa for P-PtN<sub>2</sub> is much higher than that of 22 GPa for F-PtN<sub>2</sub> along the [111] direction. These weakest links in tension are also responsible for the shear instability by the cleavagelike mode between the {100} and the {111} planes for P-PtN<sub>2</sub> and F-PtN<sub>2</sub>, respectively (see below). The minimum tensile strengths of both polymorphs are much lower than that of c-BN ( $\sim 66$  GPa (LDA) and  $\sim 55$  GPa (GGA) [45] along the weakest [111] direction).

Because plastic deformation occurs by shear, we have to study the anisotropy of the ideal shear strengths [22,29,49,45]. The lowest shear strengths of 34 GPa of P-PtN<sub>2</sub> are found for the (111)[-1-12] slip system [Fig. 2(b)]. This value is about two times higher than the lowest shear strength of 15 GPa found for F-PtN<sub>2</sub> in the (111)[11-2] slip system [Fig. 2(d)]. Thus, P-PtN<sub>2</sub> is intrinsically much stronger than F-PtN<sub>2</sub>. The lowest ideal shear strength of P-PtN<sub>2</sub> is slightly lower than that of ReB<sub>2</sub> (38 GPa (LDA) and 34 GPa (GGA) [22]) suggesting that PtN<sub>2</sub> cannot be stronger and harder than ReB<sub>2</sub> and that it is much weaker than c-BN ( $\sim 65$  GPa (LDA) and 58 GPa (GGA) [22,45]). Since the lowest shear strength of P-PtN<sub>2</sub> is still higher than that of typical hard materials, such as fcc-TiN and hcp-Si<sub>3</sub>N<sub>4</sub> [43], P-PtN<sub>2</sub> is expected to be somewhat stronger and harder than these materials.

In order to obtain a deeper understanding of the deformation paths of both PtN<sub>2</sub> polymorphs in shear, the changes in

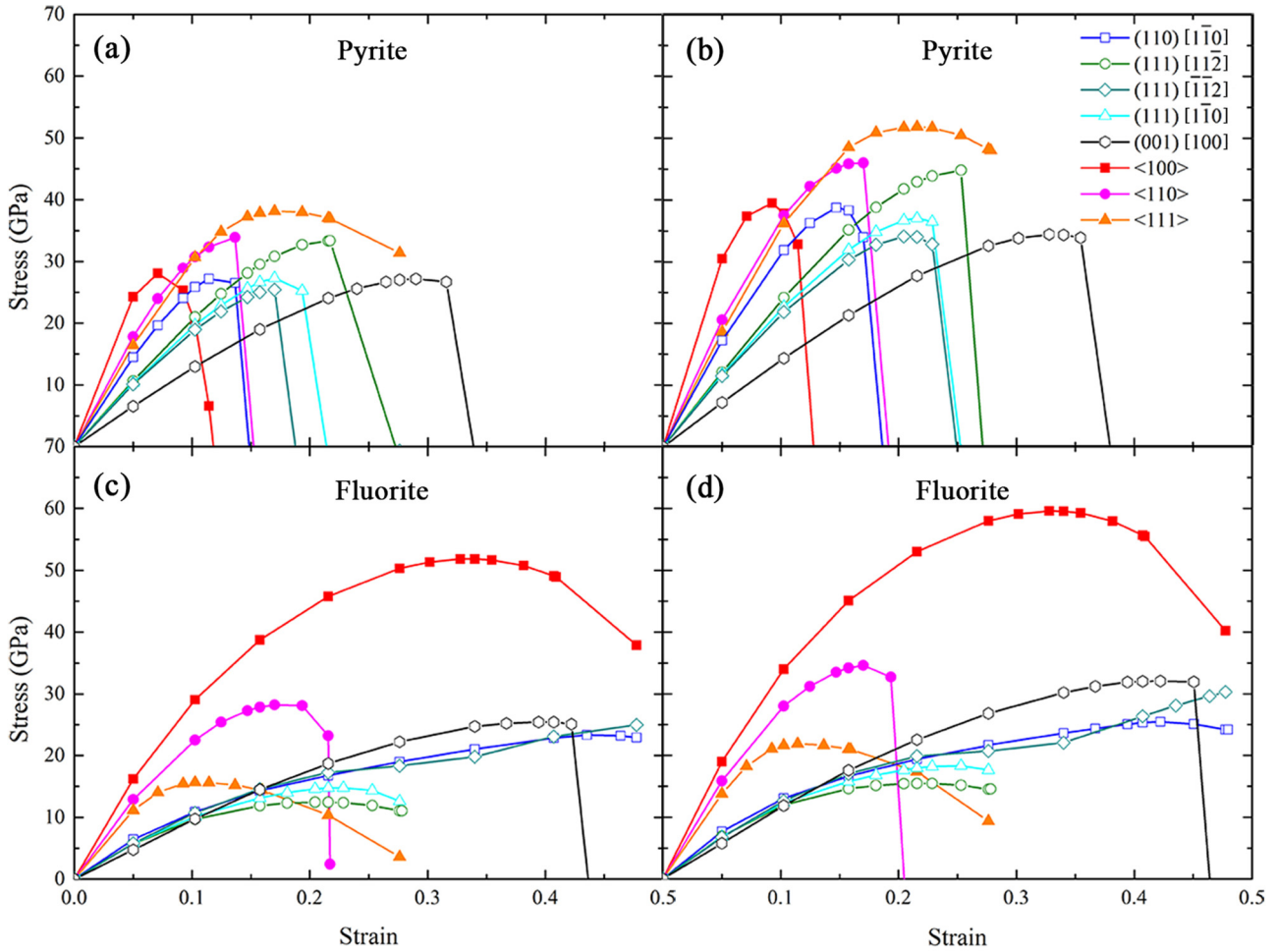


FIG. 2. (Color online) The stress-strain curves calculated for (a) P-PtN<sub>2</sub> by PAW-PBE potentials, (b) P-PtN<sub>2</sub> by PAW-LDA potentials, (c) F-PtN<sub>2</sub> by PAW-PBE potentials, and (d) F-PtN<sub>2</sub> by PAW-LDA potentials under various tension and shear deformations.

valence charge density differences (VCDDs) during shear deformation are compared in Fig. 3. (The VCDD is defined as the difference between the calculated total valence charge density of the crystal minus the valence charge densities of neutral atoms [23].) A positive value (yellow color) means an increase in the negative charge, whereas a negative value (cyan color) means its decrease as compared to neutral atoms. A higher charge density between two atoms means a stronger bond. Although both P-PtN<sub>2</sub> and F-PtN<sub>2</sub> have cubic crystal structures, their bond deformation paths and electronic instability modes are substantially different as seen from the deformed VCDD isosurfaces in Figs. 3(a) and 3(b) at the shear strains of  $\gamma = 0.2155$  (before) and  $\gamma = 0.2531$  (after instability) for P-PtN<sub>2</sub> and  $\gamma = 0.2155$  (before) and  $\gamma = 0.3400$  (after instability) for F-PtN<sub>2</sub>. For P-PtN<sub>2</sub>, the shear instability occurs between the Pt{100} planes and the N{100} planes which—after the instability—form separate flat layers of Pt and N atoms [Fig. 3(b)]. In F-PtN<sub>2</sub> however, the shear instability occurs between the Pt/N{111} planes and the N/Pt{111} planes which—after the instability—form more mixed Pt/N slabs composed of Pt and N atoms [Fig. 3(d)].

In view of the unique cleavagelike mode during shear instability, we explore now the ratio of the minimum tensile

decohesion strength ( $\sigma_{\min}$ ) to the minimum shear strength ( $\tau_{\min}$ ) for both P-PtN<sub>2</sub> and F-PtN<sub>2</sub>. The calculated ratios of  $\sigma_{\min}/\tau_{\min}$  ( $\sim 1.2$  for P-PtN<sub>2</sub> and  $\sim 1.5$  for F-PtN<sub>2</sub>) are larger than unity but lower than that of ReB<sub>2</sub> ( $\sim 1.7$  [22]). This suggests that the cleavagelike mode of shear instability under affine deformation is attributed to the tension-shear coupling [50] resolved along the weakly bonded {100} planes in P-PtN<sub>2</sub> and {111} planes in F-PtN<sub>2</sub>. In contrast to the affine deformation mentioned above [33,51], a ratio of cleavage strength to the glide strength under an alias deformation by rigid opening or sliding between two planes (e.g., Ref. [52]) may provide an alternate view of the deformation mechanism in P-PtN<sub>2</sub> and F-PtN<sub>2</sub>. This is however beyond the scope of the present paper.

To better understand the physical origin of distinct mechanical strength and the cleavagelike mode during the shear instability of both PtN<sub>2</sub> polymorphs, the electronic density of states (EDOS) are shown in Fig. 4. From Fig. 4(a) it is seen that P-PtN<sub>2</sub> shows a covalent nature with the band gap of about 1.8eV, whereas F-PtN<sub>2</sub> is metallic because of the nonzero EDOS value at the Fermi level. The small pseudogap seen at the Fermi level of the F-PtN<sub>2</sub> EDOS suggests a small covalent contribution in this case. The bonding strength can

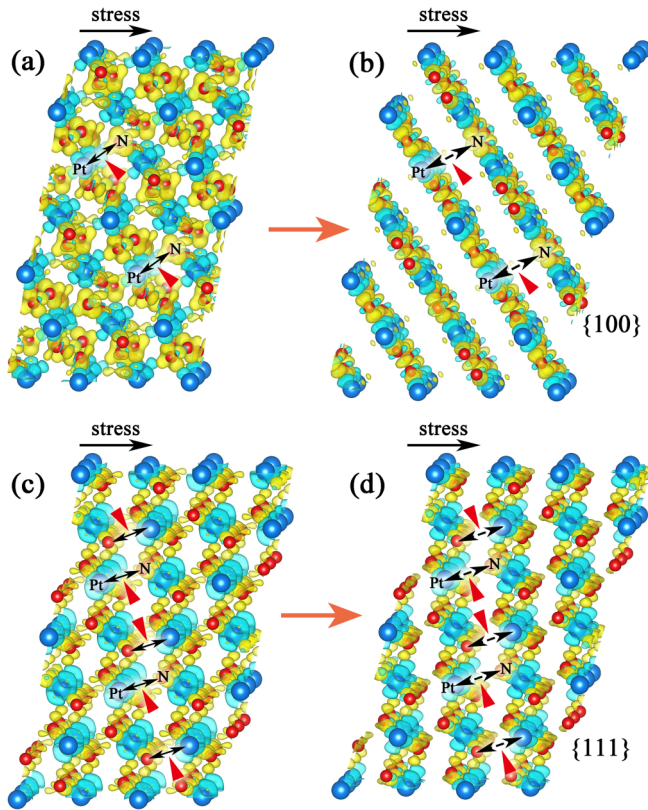


FIG. 3. (Color online) The isosurfaces of the VCDD of P-PtN<sub>2</sub> (a) before and (b) after instability under shear deformation along the weakest (111)[-1-12] slip system and those of F-PtN<sub>2</sub> (c) before and (d) after instability under shear deformation along the weakest (111)[11-2] slip system. The isosurface maps of the VCDD correspond to  $\pm 0.02 e/\text{Bohr}^3$ .

be clearly identified from the contour plot of the VCDD cross section shown in Figs. 4(c) and 4(d) for P-PtN<sub>2</sub> and F-PtN<sub>2</sub>, respectively. It is seen that the charge accumulation in the middle of the Pt-N bonds in P-PtN<sub>2</sub> [the scale of the VCDD for P-PtN<sub>2</sub> changes from  $-0.076$  to  $0.065$  in Fig. 4(c)] is much higher than that in F-PtN<sub>2</sub> [the scale of the VCDD for F-PtN<sub>2</sub> changes from  $-0.035$  to  $0.055$  in Fig. 4(d)]. This explains the electronic origin of the higher strength of P-PtN<sub>2</sub> as compared with that of F-PtN<sub>2</sub>. To quantify the charge transfer in both PtN<sub>2</sub> polymorphs, the charge-density topology is quantitatively analyzed by the quantum theory of atoms in molecules proposed by Bader [53] and Henkelman *et al.* [54]. Accordingly, the ionicity of P-PtN<sub>2</sub> and F-PtN<sub>2</sub> is determined by calculating the charge on Pt and N in the PtN<sub>2</sub> lattice to be  $\text{Pt}^{1.2167}(\text{N}^{-0.6083})_2$  and  $\text{Pt}^{1.055}(\text{N}^{-0.5342/-0.5208})_2$  for F-PtN<sub>2</sub> and P-PtN<sub>2</sub>, respectively. The higher ionicity of F-PtN<sub>2</sub> as compared with P-PtN<sub>2</sub> is in accord with its lower strengths.

#### IV. CONCLUSIONS

To summarize, the structural, thermodynamic, mechanical properties, and lattice instability modes upon deformation of

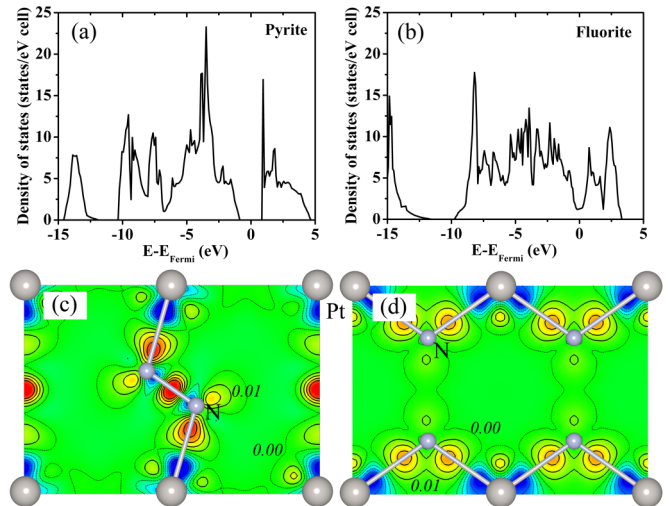


FIG. 4. (Color online) Electronic density of state for (a) P-PtN<sub>2</sub> and (b) F-PtN<sub>2</sub> and cross-sectional plot of the valence charge-density difference in (110) planes for (c) P-PtN<sub>2</sub> and (d) F-PtN<sub>2</sub>. The thick solid and thin dotted contours represent positive and negative values, respectively.

P-PtN<sub>2</sub> and F-PtN<sub>2</sub> have been presented and compared. It was shown that P-PtN<sub>2</sub> is thermodynamically more stable and significantly stronger than F-PtN<sub>2</sub>. The higher strength for P-PtN<sub>2</sub> as compared to F-PtN<sub>2</sub> is related to their different lattice topologies (the Pt-6N polyhedron and the N-N-3Pt bond topology for P-PtN<sub>2</sub>, the Pt-8N polyhedron, and the N-4Pt bond topology for F-PtN<sub>2</sub>), which in turn results in a higher covalent nature of P-PtN<sub>2</sub> as compared to the higher metallic and ionic nature of F-PtN<sub>2</sub>. The present paper shows the importance of a systematic exploration of the topology and stability of the structure, anisotropy of the elasticity and mechanical strength, chemical bonding, and electronic stability upon shear deformation when attempting to design new ultrincompressible and potentially strong and hard materials.

#### ACKNOWLEDGMENTS

R.F.Z. is supported by the Fundamental Research Funds for the Central Universities, National Natural Science Foundation of China (Grant No. 51471018), and National Thousand Young Talents Program of China. D.L. acknowledges financial and computational support by the IT4Innovations Centre of Excellence Project (Project No. CZ.1.05/1.1.00/02.0070), funded by the European Regional Development Fund, and the national budget of the Czech Republic (Project Large Research, Development and Innovations Infrastructures Project No. LM2011033). We would like to thank Professor G. Kresse for valuable advice for the application of VASP and Dr. M. Veprek-Heijman for a critical reading of the paper. S.V. thanks the SHM Company for financial support of his work.

- [1] L. E. Toth, *Transition Metal Carbides and Nitrides* (Academic, New York, 1971).
- [2] H. O. Pierson, *Handbook of Refractory Carbides and Nitrides: Properties, Characteristics and Applications* (Noyes, Westwood, NJ, 1996).
- [3] E. Gregoryanz, C. Sanoup, M. Somayazulu, J. Badro, G. Fiquet, H.-K. Mao, and R. J. Hemley, *Nature Mater.* **3**, 294 (2004).
- [4] A. F. Young, C. Sanloup, E. Gregoryanz, S. Scandolo, R. J. Hemley, and H.-K. Mao, *Phys. Rev. Lett.* **96**, 155501 (2006).
- [5] J. C. Crowhurst, A. F. Goncharov, B. Sadigh, C. L. Evans, P. G. Morrall, J. L. Ferreira, and A. J. Nelson, *Science* **311**, 1275 (2006).
- [6] Z. T. Y. Liu, D. Gall, and S. V. Khare, *Phys. Rev. B* **90**, 134102 (2014).
- [7] J. A. Montoya, A. D. Hernandez, C. Sanloup, E. Gregoryanz, and S. Scandolo, *Appl. Phys. Lett.* **90**, 011909 (2007).
- [8] Z.-j. Wu, E.-j. Zhao, H.-p. Xiang, X.-f. Hao, X.-j. Liu, and J. Meng, *Phys. Rev. B* **76**, 054115 (2007).
- [9] Z. W. Chen, X. J. Guo, Z. Y. Liu, M. Z. Ma, Q. Jing, G. Li, X. Y. Zhang, L. X. Li, Q. Wang, Y. J. Tian, and R. P. Liu, *Phys. Rev. B* **75**, 054103 (2007).
- [10] Y. X. Wang, M. Arai, T. Sasaki, and C. Z. Fan, *Phys. Rev. B* **75**, 104110 (2007).
- [11] R. Yu, Q. Zhan, and L. C. De Jonghe, *Angew. Chem. Int. Ed.* **46**, 1136 (2007).
- [12] D. Åberg, B. Sadigh, J. Crowhurst, and A. F. Goncharov, *Phys. Rev. Lett.* **100**, 095501 (2008).
- [13] A. F. Young, J. A. Montoya, C. Sanloup, M. Lazzeri, E. Gregoryanz, and S. Scandolo, *Phys. Rev. B* **73**, 153102 (2006).
- [14] A. Yildiz, U. Akinci, O. Gulseren, and I. Sokmen, *J. Phys.: Condens. Matter* **21**, 485403 (2009).
- [15] J. von Appen, M.-W. Lumey, and R. Dronskowski, *Angew. Chem. Int. Ed.* **45**, 4365 (2006).
- [16] R. B. Kaner, J. J. Gilman, and S. H. Tolbert, *Science* **308**, 1268 (2005).
- [17] R. W. Cumberland, M. B. Weinberger, J. J. Gilman, S. M. Clark, S. H. Tolbert, and R. B. Kaner, *J. Am. Chem. Soc.* **127**, 7264 (2005).
- [18] J. Haines, J. M. Leger, and G. Bocquillon, *Annu. Rev. Mater. Res.* **31**, 1 (2001).
- [19] D. He, Y. Zhao, L. Daemen, J. Qian, T. D. Shen, and T. W. Zerda, *Appl. Phys. Lett.* **81**, 643 (2002).
- [20] S. Veprek, *J. Vac. Sci. Technol. A* **31**, 050822 (2013).
- [21] H. Y. Chung, M. B. Weinberger, J. B. Levine, A. Kavner, J. M. Yang, S. H. Tolbert, and R. B. Kaner, *Science* **316**, 436 (2007).
- [22] R. F. Zhang, S. Veprek, and A. S. Argon, *Appl. Phys. Lett.* **91**, 201914 (2007).
- [23] R. F. Zhang, D. Legut, X. D. Wen, S. Veprek, K. Rajan, T. Lookman, H. K. Mao, and Y. S. Zhao, *Phys. Rev. B* **90**, 094115 (2014).
- [24] R. Mohammadi, A. T. Lech, M. Xie, B. E. Weaver, M. T. Yeung, S. H. Tolbert, and R. B. Kaner, *Proc. Natl. Acad. Sci. USA* **108**, 10958 (2011).
- [25] R. Mohammadi, M. Xie, A. T. Lech, C. L. Turner, A. Kavner, S. H. Tolbert, and R. B. Kaner, *J. Am. Chem. Soc.* **134**, 20660 (2012).
- [26] R. F. Zhang, D. Legut, Z. J. Lin, Y. S. Zhao, H. K. Mao, and S. Veprek, *Phys. Rev. Lett.* **108**, 255502 (2012).
- [27] Y. C. Liang, X. Yuan, and W. Q. Zhang, *Phys. Rev. B* **83**, 220102R (2011).
- [28] R. F. Zhang, D. Legut, R. Niewa, A. S. Argon, and S. Veprek, *Phys. Rev. B* **82**, 104104 (2010).
- [29] J. Yang, H. Sun, and C. F. Chen, *J. Am. Chem. Soc.* **130**, 7200 (2008).
- [30] F. A. McClintock and A. S. Argon, *Mechanical Behavior of Materials* (Addison-Wesley, Reading, 1966), pp. 118 and 489.
- [31] A. Kelly and N. H. Macmillan, *Strong Solids*, 3rd ed. (Clarendon, Oxford, 1986), pp. 1–56.
- [32] A. Gouldstone, K. J. Van Vliet, and S. Suresh, *Nature (London)* **411**, 656 (2001).
- [33] J. Li, K. J. Van Vliet, T. Zhu, S. Yip, and S. Suresh, *Nature (London)* **418**, 307 (2002).
- [34] K. J. Van Vliet, J. Li, T. Zhu, S. Yip, and S. Suresh, *Phys. Rev. B* **67**, 104105 (2003).
- [35] A. S. Argon, *Strengthening Mechanisms in Crystal Plasticity* (Oxford University Press, Oxford, 2008).
- [36] R. F. Zhang, S. H. Sheng, and S. Veprek, *Scr. Mater.* **68**, 913 (2013).
- [37] X. H. Yu, R. F. Zhang, D. Weldon, S. C. Vogel, J. Z. Zhang, D. W. Brown, Y. B. Wang, H. M. Reiche, S. M. Wang, S. Y. Du, C. Q. Jin, and Y. S. Zhao, *Sci. Rep.* **5**, 12552 (2015).
- [38] G. Kresse and J. Furthmüller, *Comput. Mater. Sci.* **6**, 15 (1996).
- [39] G. Kresse and D. Joubert, *Phys. Rev. B* **59**, 1758 (1999).
- [40] J. P. Perdew, K. Burke, and M. Ernzerhof, *Phys. Rev. Lett.* **77**, 3865 (1996).
- [41] K. Parlinski, Z. Q. Li, and Y. Kawazoe, *Phys. Rev. Lett.* **78**, 4063 (1997).
- [42] A. Togo, F. Oba, and I. Tanaka, *Phys. Rev. B* **78**, 134106 (2008).
- [43] R. F. Zhang, S. H. Sheng, and S. Veprek, *Appl. Phys. Lett.* **90**, 191903 (2007).
- [44] R. F. Zhang, S. H. Sheng, and S. Veprek, *Appl. Phys. Lett.* **91**, 031906 (2007).
- [45] R. F. Zhang, S. Veprek, and A. S. Argon, *Phys. Rev. B* **77**, 172103 (2008).
- [46] R. Yu, Q. Zhan, and X. F. Zhang, *Appl. Phys. Lett.* **88**, 051913 (2006).
- [47] R. Yu and X. F. Zhang, *Appl. Phys. Lett.* **86**, 121913 (2005).
- [48] S. F. Pugh, *Philos. Mag.* **45**, 823 (1954).
- [49] V. V. Brazhkin, A. G. Lyapin, and R. J. Hemley, *Philos. Mag. A* **82**, 231 (2002).
- [50] N. Nagasako, R. Asahi, and J. Hafner, *Phys. Rev. B* **85**, 024122 (2012).
- [51] M. Jahnátek, J. Hafner, and M. Kráží, *Phys. Rev. B* **79**, 224103 (2009).
- [52] P. Lazar, X. Q. Chen, and R. Podloucky, *Phys. Rev. B* **80**, 012103 (2009).
- [53] R. F. W. Bader, *Atoms in Molecules—A Quantum Theory* (Oxford University Press, Oxford, 1990).
- [54] G. Henkelman, A. Arnaldsson, and H. Jónsson, *Comput. Mater. Sci.* **36**, 354 (2006).